Fuel 392 (2025) 134862

Contents lists available at ScienceDirect

Fuel

journal homepage: www.elsevier.com/locate/fuel

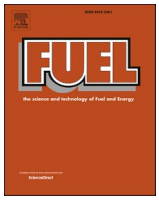

Full Length Article

Study on the effect of biochar catalyst on the formation of biomass slow pyrolysis products

Jishuo Li [a,b], Kaili Xu [a,b,*], Xiwen Yao [a,b], Jia Liu [a,b,c], Dengke Su [a,b], Bingchen Wang [a,b]

[a] School of Resources and Civil Engineering, Northeastern University, Shenyang 110819, PR China
[b] Key Laboratory of Ministry of Education on Safe Mining of Deep Metal Mines, Shenyang 110819, PR China
[c] School of Energy and Water Resources, Shenyang Institute of Technology, Fushun 113122, PR China

ARTICLE INFO

Keywords:
Biochar
O-containing functional group
Catalyst
Tar conversion efficiency
Catalytic activity

ABSTRACT

The use of solid products from biomass pyrolysis as catalysts and the analysis of the generation patterns of catalytic products are of great significance for clean energy production. This paper primarily examines the key role of the physicochemical properties of biochar in reducing tar yield and increasing syngas production. The results show that the rich O-containing functional groups and developed pore structures on the surface of biochar are good for catalyst catalyzed tar reforming for hydrogen production. Among the three biochars, corn stalk biochar has the highest tar conversion efficiency at the catalytic temperature of 800℃. The introduction of biochar catalysts can convert tar into small organic molecules and combustible gases. After catalysis, the amount of O-containing organics in tar is much smaller. The organics containing only C and H, such as naphthalene, phenanthrene, and pyrene, are the main organic components. Increasing catalytic temperature or catalyst mass increases tar conversion efficiency and relative content of H_2. Activation of the samples with activators KOH and H_3PO_4 yield catalysts with larger specific surface area, more developed pore structures, richer O-containing functional groups, and higher catalytic activity. Activation with H_3PO_4 by one step and two step methods obtain a tar conversion efficiency of 72.31% and 70.83%.

1. Introduction

Tar, as a byproduct of biomass pyrolysis composed mainly of polycyclic aromatic compounds, is easily condensed during real production to clog and corrode downstream equipment, affecting environmental production and human health. As presence of tar also reduces energy conversion efficiency during pyrolysis, many studies have focused on tar cracking and catalytic reforming to ensure best utilization of this part of energy. In order for tar to crack into combustible gases, the reactor temperature is normally set to 1000℃ or higher, resulting in low efficiency at high energy consumption [1].

To avoid high energy consumption associated with high temperature reaction conditions, using catalysts to convert tar into syngas has proved to be an effective way of improving energy conversion efficiency. And the hydrogen gas generated by catalysis has multiple uses as a clean energy [2,3]. Le *et al.* [4] emphasized the importance of increasing hydrogen production for the development of future energy development technologies. Abdelhamid [5] summarized the various hydrogen production methods and highlighted the challenges of hydrogen production and utilization in the future. Panchenko *et al.* [6] compared hydrogen production technologies in several countries and found that hydrogen production is one of the important ways to develop clean energy in the future. More and more research is focusing on hydrogen energy. In the process of biomass pyrolysis, in order to obtain more hydrogen, many researches have developed and prepared catalysts that can reduce the biomass tar and improve the hydrogen yield. It can be seen that the study of biochar catalytic biomass tar reforming for hydrogen production is very important for the development of hydrogen energy.

With high specific surface area, impressive pore area, impressive thermal stability and rich functional group structures, biochar has been proved in many studies to be effective in removing tar and increasing the content of combustible components in syngas [7–9]. Wang *et al.* [10] prepared different types of biochar to reform gaseous products from biomass pyrolysis. In addition to reducing tar yield, biochar can also promote the generation of H_2. When examine the effect of biochar on tar

* Corresponding author at: School of Resources and Civil Engineering, Northeastern University, Shenyang 110819, PR China.
E-mail address: xkl_safety@163.com (K. Xu).

https://doi.org/10.1016/j.fuel.2025.134862
Received 26 December 2023; Received in revised form 25 September 2024; Accepted 19 February 2025
Available online 27 February 2025

catalytic cracking, Song *et al.* [11] discovered that increasing the strength of O-containing functional groups on the surface of biochar boosts tar catalytic reforming; O-containing functional groups participate in the catalytic cracking. Singh *et al.* [12] investigated the tar catalysis mechanism of biochar through experimental studies and found that, as the active site of catalytic reaction, the O-containing groups in biochar facilitate the cracking and reforming of heavy tar into smaller aromatics and aliphatic fragments and will react with radicals in the biochar to generate syngas. Wijitkosum [13] discussed the effects of pyrolysis temperature and retention time on the physicochemical properties of disposable bamboo chopstick biochar. They found that biochar aromaticity increased significantly with increasing temperature and retention time. The morphology and surface functional groups of biochar can be modified by physical or chemical activation processes to further improve its activity during tar catalysis [14]. Peng *et al.* [15] impregnated pine sawdust biochar in 47.5 % H_3PO_4 solution at the mass ratio of 1: 1 for 24 h and dried and activated it. The specific surface area of biochar increased from 408 m^2/g to 900 m^2/g. When examining H_3PO_4 and $ZnCl_2$ activated olive stones, Nakagawa *et al.* [16] discovered that H_3PO_4 prepared biochar contains more mesopores and micropores, whereas $ZnCl_2$ prepared biochar contains mainly micropores. So far, most studies on biochar activation have been concentrated more on the effects of activation conditions on the specific surface area, pore size, surface functional group structure and micro morphology of biochar. Little has been reported on how modified biochar can be used in tar catalytic cracking, especially how biochar activation affects tar composition, tar conversion efficiency, and syngas generation.

This study aims to examine how biochar affects tar generation and syngas release when catalyzing the pyrolysis of biomass into gaseous products. First, the effects of biochars from pyrolysis of different biomasses and their catalytic conditions—including catalytic temperature and catalyst mass—on tar conversion efficiency and syngas release curves are instigated. Then, biochars are activated and modified with different activators and by activation methods to observe how modified biochars affect tar conversion efficiency and syngas release curves. The catalysis mechanism of biochar is analyzed by comparing catalytic performance, functional group structures and micro morphology before and after activation and catalysis.

2. Experimental method and theory

2.1. Preparing catalysts

Biochars obtained from pyrolysis of corn stalk, wheat stalk, and poplar sawdust were used as catalysts for tar catalytic reforming. The biochars used for our experiment were prepared at the N_2 flow of 0.3 L/min and heating rate of 10℃/min. After they were heated to a given temperature, they were held for 60 min to ensure full carbonization. The three biochars are noted as CS-BC, WS-BC, and PS-BC. During experiment, wheat stalk was used as the pyrolysis raw material.

In order to further improve the catalytic activity of biochar, chemical activation was applied to prepare biochars with higher catalytic activation. KOH and H_3PO_4 were selected as the basic activator and acid activator, respectively. Both activators were sourced from Shanghai Macklin Biochemical Co., Ltd. Biochars were prepared by one step and two step activation methods. One step activation was implemented in the following steps: weigh 10 g of KOH and place it into a breaker containing 200 mL deionized water, stir it in a magnetic stirred for 15 min until it is fully dissolved. Take 10 g of the biomass raw material, pour it slowly into the breaker, stir continuously for 4 h and keep for 24 h. After impregnation, stir in the magnetic stirrer at 80℃ until there is little residual moisture and then dry in a vacuum dryer at 105℃ for 36 h. After the sample is completely dry, heat it to 800℃ in a tubular furnace at the N_2 flow of 0.3 L/min and heating rate of 10℃/min, hold for 60 min until it is naturally dried and then take out the sample. In order to remove the K ions in the sample, prepare 0.1 mol/L HNO_3 solution to clean the sample, then wash it with deionized water until the pH of the filtrate is 7. Dry the cleaned sample at 105℃ for 48 h, sieve it through a 100-mesh sieve to obtain KOH-activated biochar. H_3PO_4 activation is similar to KOH activation: the amount of H_3PO_4 is also 10 g, except that the sample prepared at 800℃ is directly washed with deionized water to pH = 7. These two catalysts are noted as KBC and HBC. Two step activation is similar to one step activation, except that the activator-impregnated sample is biochar from pyrolysis at 500℃: first, heat the biomass raw material to 500℃ in a tubular furnace at the N_2 flow of 0.3 L/min and heating rate of 10℃/min, hold for 30 min until it is dried naturally and take it out. Then, obtain biochars needed for the experiment by impregnation, drying and pyrolysis. The H_3PO_4 prepared catalyst by two step activation is noted as HBC-2.

2.2. Experimental method

Fig. S1 shows the biomass pyrolysis-catalysis experiment flowchart. The quartz tube has an outer diameter of 60 mm and a wall thickness of 4 mm. The heating length of the pyrolysis section on the left and the catalysis section on the right of the tubular furnace is both 300 mm. In each experiment, 10 g of wheat stalk was weighed and placed in the pyrolysis section on the left; a given amount of catalyst was weighed and placed in the catalysis section on the right, in the middle of the heating section. As catalyst was powdered, it was spread evenly on quartz wool and then put into the catalysis section of the tubular furnace. During experiment, the catalysis section was heated first at the N_2 flow of 0.2 L/min and heating rate of 10℃/min up to a given temperature and then held all the time. Next was the heating of the pyrolysis section, which was heated at the N_2 flow of 0.2 L/min and heating rate of 10℃/min up to 800℃ and held for 60 min. A gas analyzer was used to monitor and record the relative volume fraction variation of the syngas components generated during experiment at the data acquisition frequency of 10 times/min. The tar collected in the condenser unit was evaporated, purified and weighed with a rotary evaporator before it was collected into a sample bottle and kept under 5℃ for further test.

2.3. Characterization method

The elements in the biochar samples were qualitatively and quantitatively analyzed by X-ray fluorescence spectrometry (XRF), using A ZSX Primus II X-ray fluorescence spectrometer (Rigaku, Japan). The structures and relative contents of functional groups in different biochars were analyzed by X-ray photoelectron spectrometry (XPS), using A Thermo SCIENTIFIC K-Alpha X-ray photoelectron spectrometer. The type and relative strength of functional groups in the biochars were analyzed by Fourier transform infrared spectroscopy (FTIR), using a VERTEX 80 FTIR analyzer (Bruker, Germany). The crystal structure of the biochars was analyzed by X-ray diffraction (XRD) at 5–90°, using an X Pertpro X-ray diffractometer (Panalytical, Netherlands). The micromorphology and surface elements of the biochars were analyzed by scanning electron microscopy (SEM) and X-ray energy dispersive spectrometry (EDS), using an Ultra Plus field emission scanning electron microscope (Zeiss, Germany) and a QUANTAX 200 energy dispersive spectrometer (Bruker, Germany). The composition of the tar collected after catalysis was analyzed by gas chromatography-mass spectrometry (GC–MS), using an Aligent 8860-5977B GCD.

2.4. Chemical reactions during pyrolysis and catalysis

Table S1 lists the main reactions involved in biomass pyrolysis and tar catalytic reforming. The former mainly involves dehydration, devolatilization, and decomposition of residue carbon and inorganics, during which gaseous products and solid products are produced. When they pass the catalysis section, gaseous products, such as O-containing organics, hydrocarbon organics, water, CO_2, and CH_4, will be chemically reacted to generate organics and small molecule gases such as CO, CH_4,

and H_2; gaseous products also generate high molecule gases when cracking under high temperature. When biochar catalyzes tar reforming, it not only provides active sites, but also participates in the catalytic reforming reaction [17]. Hence biochar type, mass ratio between biochar and raw material, catalytic temperature, and residence time can also make a difference to tar yield and syngas composition. From Table S1, the tar organics from biomass pyrolysis and the catalytically reformed CO_2 can facilitate the generation of CO and H_2. Also, as tar cracking is an endothermic reaction, high temperature catalysis is good for tar cracking and reforming, thus facilitating the generation of CO and H_2.

3. Results and discussion

3.1. Physiochemical properties of biochar

3.1.1. Chemical composition of different biochars

Table 1 lists some of the oxides in the biochar samples used for tar catalysis experiment and their relative contents from XRF analysis. The biochars contain transition metals Fe and Mn, alkali metals K and Na, and alkaline-earth metals Ca and Mg. In all three biochars, the contents of K_2O and CaO are higher than other metal oxides; the content of Na_2O is very low. The contents of these three oxides are 0 %, 0.07 %, and 0.05 %. Presence of alkali and alkaline-earth metal (AAEM) elements boosts tar catalytic reforming and can improve the catalytic activity of biochar. Besides AAEM elements, presence of Fe in biochar also contributes positively to tar catalytic reforming. The relative contents of Fe_2O_3 in the three biochars are 0.15 %, 1.50 %, and 0.27 %. Some studies have indicated that during catalysis, Fe can improve the anti-coking performance, and consequently the stability of the catalyst [18].

3.1.2. Functional group structure of different biochars

Fig. S2 compares the XPS patterns and peak fitting plots of Cls and Ols for CS-BC before and after catalysis. Peak fitting of Cls yielded five peaks. The peak at 284.8 eV indicates presence of C-C or C-H structures in the aromatic units and their substituted alkanes; the peak at 286 eV indicates presence of C-O structures in phenols, alcohols, or ethers; the peak at 286.9 eV indicates presence of C=O structures; that at 288.8 eV indicates presence of O=C-O structures. Peak fitting of Ols yielded three peaks. The O-containing functional groups at 530.2 eV, 532 eV, 533.8 eV, and 535.2 eV are C=O, C-O in O=C-O, O=C-O or C-O, and -COOH. Affected by adjacent atoms, the peak position of the same functional group is slightly different among different biochar samples [19].

The relative contents of Ca, O, and C in the biochars were measured by XPS. From the diagrams, after activation, the relative content of O in the biochar is much higher, suggesting that the activator can enrich the O-containing functional groups on the surface of the biochar catalyst, and one-step activation is more able to help increase the relative content of O in the biochar. Comparison of the relative content of O in the biochar before and after activation and catalysis indicates that the relative content of O is reduced a little. The O-containing compounds in the biochar may have participated in the catalytic reaction. Also, the O-containing functional groups in the biochar are primarily C-O; after activation and catalysis, the relative contents of all functional groups in the biochar have changed. During tar catalytic cracking, the O-containing functional groups in the biochar helped decompose large molecule organics and facilitated the catalytic reaction. When examining biochar-catalyzed biomass pyrolysis, Yang *et al.* [20] discovered that -OH, O=C-O, and C-O functional groups have high catalytic activity; during pyrolysis and catalysis, they not only facilitate tar cracking, but also participate in the catalytic cracking as reactants. When studying the use of biochar as a catalyst for tar steam reforming, Liu *et al.* [21] also found that the C-O structures in aromatic organics play a critical role in catalytic cracking and C-O functional groups can participate in tar reforming as an active intermediate. In light of the XPS analysis results in the diagrams, introduction of an activator can probably improve the catalytic activity of biochar activators.

Fig. 1 compares the FTIR patterns of different biochars before and after catalysis. The functional group structures of the three biochars and the activated biochars are similar despite strength differences, with CS-BC functional groups being stronger than WS-BC and PS-BC. In CS-BC, the C-O functional groups are stronger than the other functional groups, which agrees with the XPS analysis result. The absorption peak at 3700–3100 cm^{-1} results from the stretching vibration of -OH in water, phenol, acid, or alcohol. From the diagrams, after KOH and H_3PO_4 activation, the -OH structures on the surface of all biochars has been enhanced to different degrees. The absorption peaks at 1200–1000 cm^{-1} and 900–700 cm^{-1} indicate the stretching vibration of C-O and aromatic C-H bonds. After activation, all these functional groups have become stronger.

The functional group structures of biochars prepared by one step activation (HBC) and two step activation (HBC-2) are similar, but the strength of the absorption peaks of C-O and C-H in HBC are stronger, suggesting that the O-containing functional groups on the surface of biochar prepared by one step activation are richer, which agrees with the XPS analysis result. As the main active sites, O-containing functional groups played a critical role in tar catalytic cracking; rich active sites help adsorb organics and facilitate tar cracking. Also, as reactants, O-containing functional groups reacted with organics to generate smaller molecule aromatic or hydrocarbon organics [22]. From the diagrams, after reaction, the functional groups in the biochars are all weaker, suggesting that during catalysis, -OH and C-O structures participated in the reaction and weakened the strength of the functional groups. After catalysis, the absorption peak of -OH functional groups in KBC is much

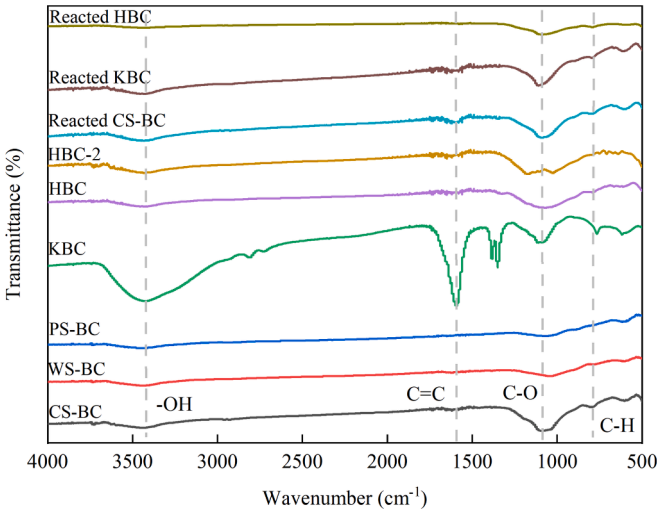

Fig. 1. FTIR patterns of the biochar samples.

Table 1
XRF analysis result of the biochar samples.

Oxidant (wt%)	SiO_2	K_2O	P_2O_5	CaO	MgO	MnO	Al_2O_3	Fe_2O_3	Na_2O
CS-BC	73.96	3.09	1.59	0.96	0.73	0.34	0.28	0.15	0
WS-BC	35.64	15.30	1.95	5.14	1.62	0.49	4.54	1.50	0.07
PS-BC	5.66	1.80	0.34	2.86	0.76	0.02	2.08	0.27	0.05

lower. During tar catalytic cracking, -OH structures must have reacted with the organics and facilitated the generation of H_2.

3.1.3. Crystal structure of different biochars

Fig. 2 compares the XRD patterns of CS-BC, KBC, HBC, and reacted CS-BC. There is a strong and broad diffraction peak between 20°1–25°, attributable to amorphous carbon structure C(002), which in a way reflects the graphitization degree of the sample. After KOH and H_3PO_4 activation, this same diffraction peak in the crystal structure of the biochar becomes weaker, suggesting that the activator caused a disruption to the graphitized structure. Another diffraction peak indicative of the graphitilization degree of samples falls between 40°–50°, attributable to presence of graphite structure C. From the diagrams, after activation, this diffraction peak in the biochar is slightly lower. In the standard XRD pattern of graphite, there are nine high strength characteristic peaks of graphite—(002), (100), (101), (004), (102), (103), (110), (110), and (006). In the diagrams, the sample has only two characteristic diffraction peaks of graphite, suggesting that the sample is less graphitized and its structure is highly disordered. After activation, the biochar is less graphitized and microcrystallized, which facilitates the development of pores in the biochar structure.

3.1.4. Effect of activator on biochar pore structure

Table 2 gives the pore structure of CS-BC and activated biochar. After pyrolysis, the specific surface area and total pore volume of the KOH and H_3PO_4 activated biochars are much larger. The specific surface area increased from 7.758 m^2g^{-1} to 58.744 m^2g^{-1} and 31.255 m^2g^{-1}; the total pore volume increased from 0.051 cm^3g^{-1} to 0.241 cm^3g^{-1} and 0.137 cm^3g^{-1}. After activation, the average pore size is lower, dropping from 26.546 nm to 16.441 nm and 19.426 nm. Large mesopore structures make it convenient for the organic molecules in tar to contact the active sites on the surface of biochar; it will also increase the contact time between organics and biochar [23]. Xu *et al.* [24] revealed that the mesopore structures in catalyst carriers are adsorptive enough to effectively convert large molecule organics into small molecule organics and combustible gases. On this basis, biochar catalysts prepared by one step activation should have higher catalytic activity.

Fig. 3 compares the SEM images of CS-BC, KBC, and HBC. Table S2 gives the distribution and relative contents of elements near the surface pore structures of the biochars. From the images, CS-BC is honeycomb shaped with irregular pore structures over the surface. On the surface of the activated KBC and HBC, even more pore structures appear; the surface pores of the H_3PO_4 activated biochar are even larger in size. From Table S2, the activated biochars have lower C and higher O. In the KOH activated KBC, although K has been removed by acid wash, there is still some K, with a content of 2.71 %. In the H_3PO_4 activated HBC, the content of P is much higher, too, increasing from 0.97 % to 6.95. These two elements can contribute positively to tar catalytic cracking [25]. The C content in KBC is reduced because during activation, C has undergone a series of chemical reactions with KOH to generate K_2CO_3 and thus produced many micropore structures on the surface of KBC. Formation of micropore structures is also related to the etching effect of biochar. During pyrolysis, KOH will inhibit the generation of tar. This reduces the chance of tar clogging fine pores and facilitates the generation of micropore structures [26]. Many pore structures appear on the surface of HBC possibly because, on the one hand, the phosphate generated from H_3PO_4 reaction facilitated the expansion of biomass structures during pyrolysis to form more pore structures; on the other hand, the catalytic degradation effect of H_3PO_4 caused the biomass precursor to become lower molecules and volatilize in the form of gas to form more pore structures [27,28].

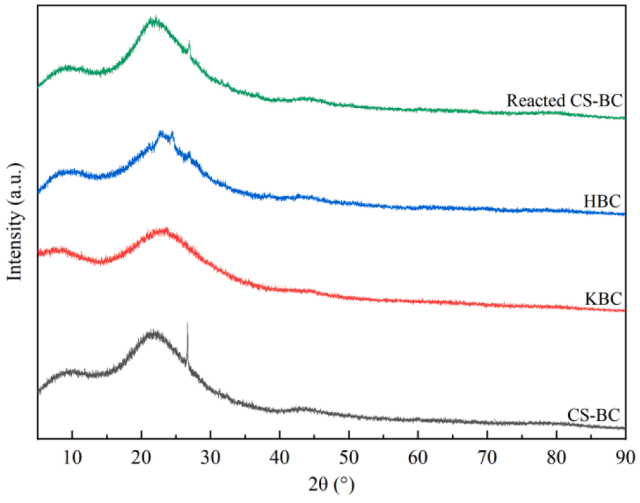

Fig. 2. XRD patterns of the biochar samples.

Table 2
BET specific surface area analysis of the biochar samples.

	$S_{BET}(m^2g^{-1})$	$V_T(cm^3g^{-1})$	D_A(nm)
CS-BC	7.758	0.051	26.546
KBC	58.744	0.241	16.441
HBC	31.255	0.137	19.426

3.2. Catalysis experiment results of biochar

3.2.1. Effect of catalytic temperature on pyrolysis product

Fig. 4 describes how tar conversion efficiency changes with catalytic temperature when CS-BC is used as the catalyst at the mass of 5 g. Catalytic temperature affects tar conversion efficiency in roughly the same way with and without biochar; higher catalytic temperature helps reduce tar yield. Without biochar, as catalytic temperature increases, tar conversion efficiency increases from 58.01 % to 63.44 %. This suggests that tar yield will greatly reduce under higher catalytic temperature even when no catalyst is added. Under high temperature, the organics in tar will undergo a series of reactions like demethylation, branched chain breaking, and intramolecular bridge bond breaking, which further converts tar into small molecule gases and organics [29]. From the diagram, after adding biochar in the catalysis section, the tar conversion efficiency is much higher. The tar removal of biochar typically involves adsorption and catalytic cracking. During adsorption, the rich pore structures in the biochar adsorb tar onto the active sites of the biochar. Subsequent catalytic cracking cracks the organics in tar into smaller molecule organics and generates combustible gases like H_2 and CO [12]. Furthermore, it has been demonstrated that higher catalytic temperature and presence of biochar can facilitate guaiacol organics to generate phenolic organics and small molecule gases through demethoxy reaction, thus reducing the cracking activation energy of tar and boosting the breaking of C-C and C-H bonds therein [30].

Fig. 5 describes how catalytic temperature affects syngas without biochar. Under the three catalytic temperatures, the maximum values of the H_2 release curve are 6.26 %, 12.80 %, and 25.10 %. The value of H_2 release curve increases by almost one-fold for every 100℃ increase. When the catalytic temperature is 900℃, the maximum value of the H_2 release curve is larger than that of the CO release curve; the H_2 release curve stays above the CO release curve almost throughout the pyrolysis. At the pyrolysis time of 75–85 min, another obvious peak—9.25 %, 10.25 %, and 11.54 %—appears. At this point the peak increases with increasing catalytic temperature, but at a very small rate compared with the first peak. Park *et al.* [31] found that at 700℃, CH_4 will be reformed into H_2 and CO, as is confirmed by the variation of CO release curves here. Catalytic temperature does not make much difference to the maximum value of the CO release curve. Under the three catalytic temperatures, the maximum values are 24.54 %, 24.52 %, and 23.59 %, and they drop a little with increasing catalytic temperature. As with CO,

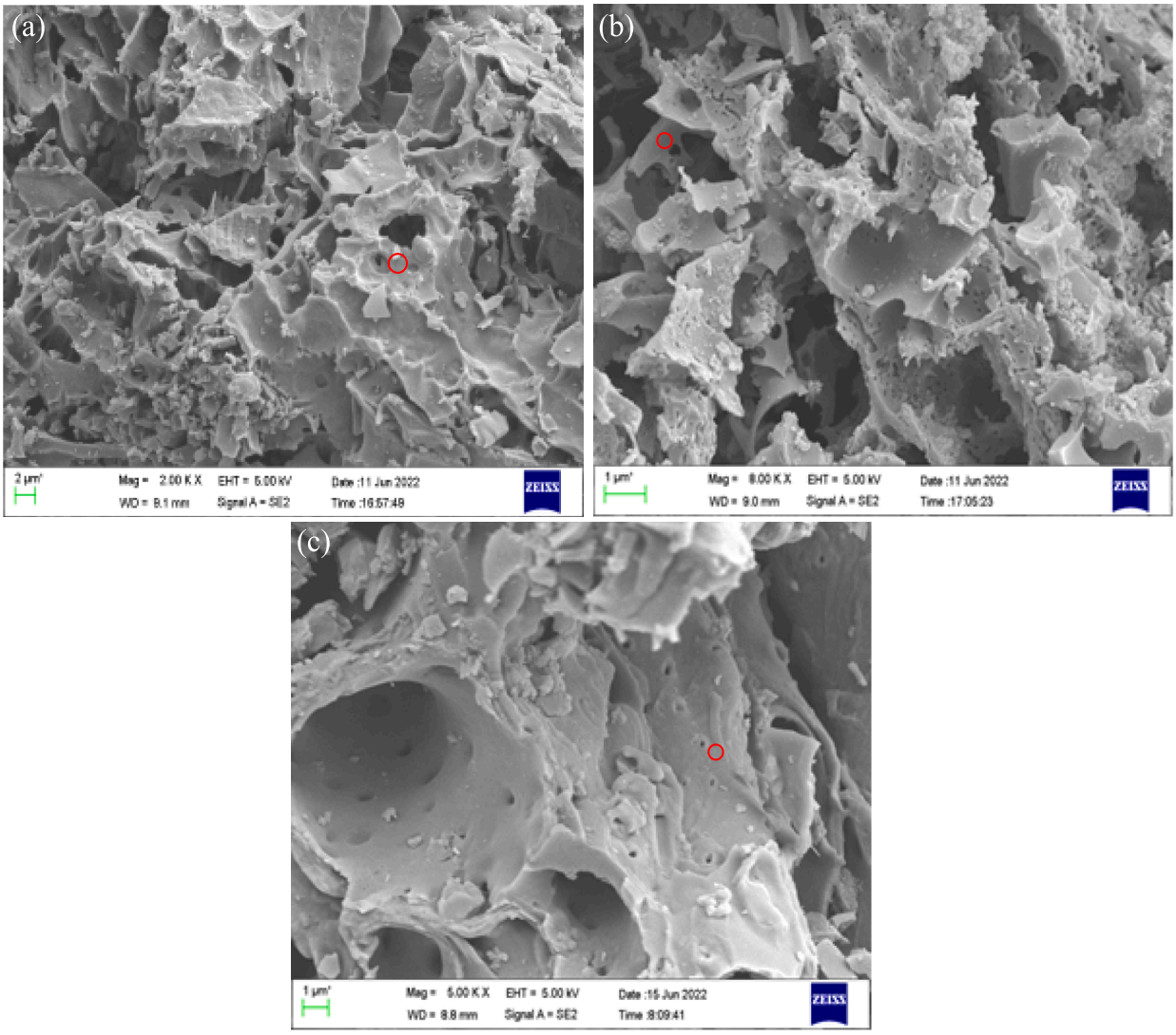

Fig. 3. SEM images of (a) CS-BC, (b) KBC, and (c) HBC.

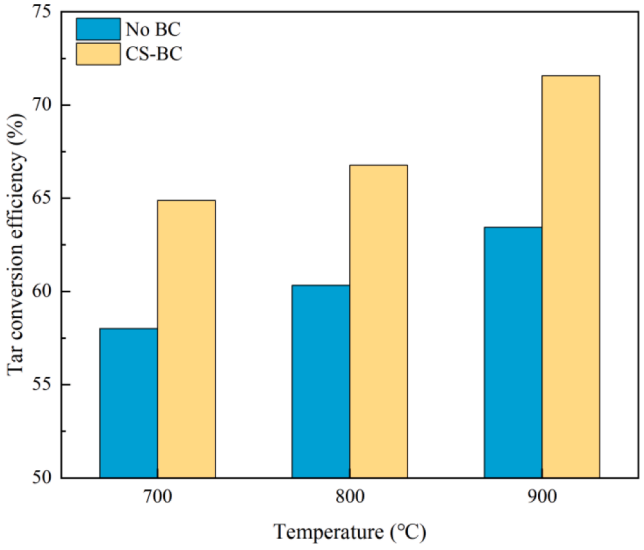

Fig. 4. Tar conversion efficiency as a function of catalytic temperature.

catalytic temperature makes little difference to the maximum value of the CO_2 release curve. Under the three catalytic temperatures, the maximum values are 12.61 %, 13.92 %, and 11.66 %. When the catalytic temperature increases from 700℃ to 800℃, the maximum value of CH_4 does not change much. When the catalytic temperature increases to 900℃, the maximum value of the CH_4 release curve changes obviously. The relative content of CH_4 is reduced mainly due to steam reforming of methane and the cracking of methane itself into H_2.

Fig. 6 describes how catalytic temperature affects syngas with 5 g CS-BC catalyst. Presence of biochar simply affects syngas yield but does not make much difference to the variation of syngas with temperature. This is mainly because the role of biochar is to facilitate the gaseous product from decomposition of wheat stalk to further crack and reform into syngas, namely, it boosts the chemical reactions of (2)– (10) in Table S1, but does not affect the decomposition of the biomass itself. Compared with when no biochar is used, biochar greatly facilitates the generation of H_2 under all catalytic temperatures. The maximum values of the H_2 release curve increase from 6.26 %, 12.80 %, and 25.10 % to 11.02 %, 21.42 %, and 27.42 %; the second peaks of the H_2 release curve change from 9.25 %, 10.25 %, and 11.54 % to 9.22 %, 9.94 %, and 11.99 %. At this point, the peak values are not much different from when no biochar is added, suggesting that the experimental conditions for the catalysis section did not affect the appearance of the second peak value. From the

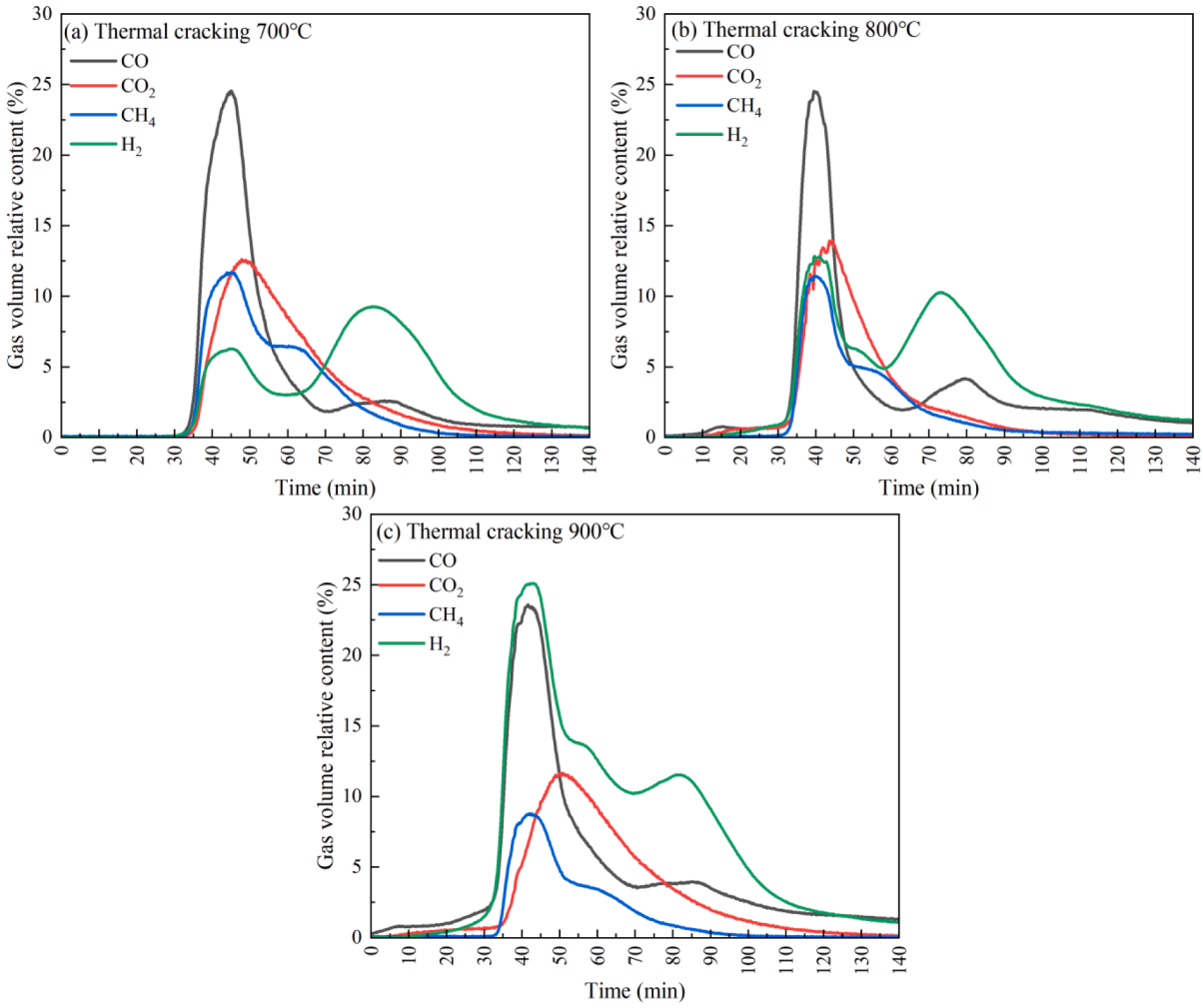

Fig. 5. Effect of catalytic temperature on syngas release curves without biochar.

plots, catalytic temperature affected the generation of CO and CO_2 less significantly as it did H_2. Increased catalytic temperature reduced the relative content of CH_4 in the syngas. Similar to when no biochar was used for catalysis, as CH_4 was cracked into H_2 under high temperature, the maximum value of the CH_4 release curve dropped significantly when the temperature increases from 800℃ to 900℃.

In order to understand how catalytic temperature affects content of syngas components, the first 1050 data points monitored for each group of experiment were summed and plotted into Fig. 7. The data point sums of syngas curves were normalized and given in Table S3. The data point sums of syngas components under different temperatures reflect in a way how yield of syngas components changes with catalytic temperature. From Fig. 7 and Table S3, as catalytic temperature increases, the relative content of H_2 in the syngas increases obviously; presence of biochar also greatly increases the relative content of H_2 in the syngas. As catalytic temperature increases, the relative content of CO in the syngas increases, too, but increase of catalytic temperature or addition of biochar does not affect the relative content of CO in the syngas so much. Unlike the release pattern of H_2 and CO, with the increase of catalytic temperature or addition of biochar, the relative contents of CO_2 and CH_4 from pyrolysis are both reduced to a degree.

3.2.2. *Effect of biochar mass on pyrolysis product*

Fig. 8 shows how biomass tar conversion efficiency changes with biochar mass at the catalytic temperature of 800℃. As biochar mass increases from 5 g to 15 g, tar conversion efficiency increases from 66.77 % to 79.21 %, suggesting that increase of biochar mass is conducive to tar cracking. Tar conversion efficiency is increased because, on the one hand, increase of active sites on the surface of biochar reduced the activation energy needed for tar cracking, making it easier for tar to crack; on the other hand, increase of biochar mass provided longer reaction time for tar catalytic reforming, further intensifying tar cracking and reforming.

Fig. 9 shows how the syngas release curve of wheat stalk changes with pyrolysis time of at different biochar masses. When biochar mass increases from 5 g to 15 g, the H_2 release curve changes obviously. Under the three catalytic conditions, the first peak values of the H_2 release curve are 21.42 %, 24.17 %, and 22.96 %; the peak values at 75–85 min are 9.94 %, 10.24 %, and 12.24 %. The H_2 release curve at 15 g biochar mass is obviously wider than at 5 g biochar. Obviously, increase of biochar mass facilitated the generation of H_2. Increase of biochar mass greatly affected the CO release curve, too—the peak values are 24.21 %, 26.96 %, and 25.14 %. Similar to the H_2 release curve, when the biochar mass increases to 15 g, the CO release curve is obviously wider, suggesting that increase of biochar mass facilitated the generation of CO.

Fig. 10 shows the sums of the first 1050 data points of syngas components monitored by the gas analyzer during the catalysis experiment at different biochar masses. Table S4 gives the relative contents of syngas components normalized from their respective data point sums at different biochar masses. From the diagram, as biochar mass increases, the data points sum of H_2 and CO increases significantly; that of CH_4 and CO_2 does not change much and reduces a little instead, suggesting that increase of biochar mass facilitated the generation of H_2 and CO but

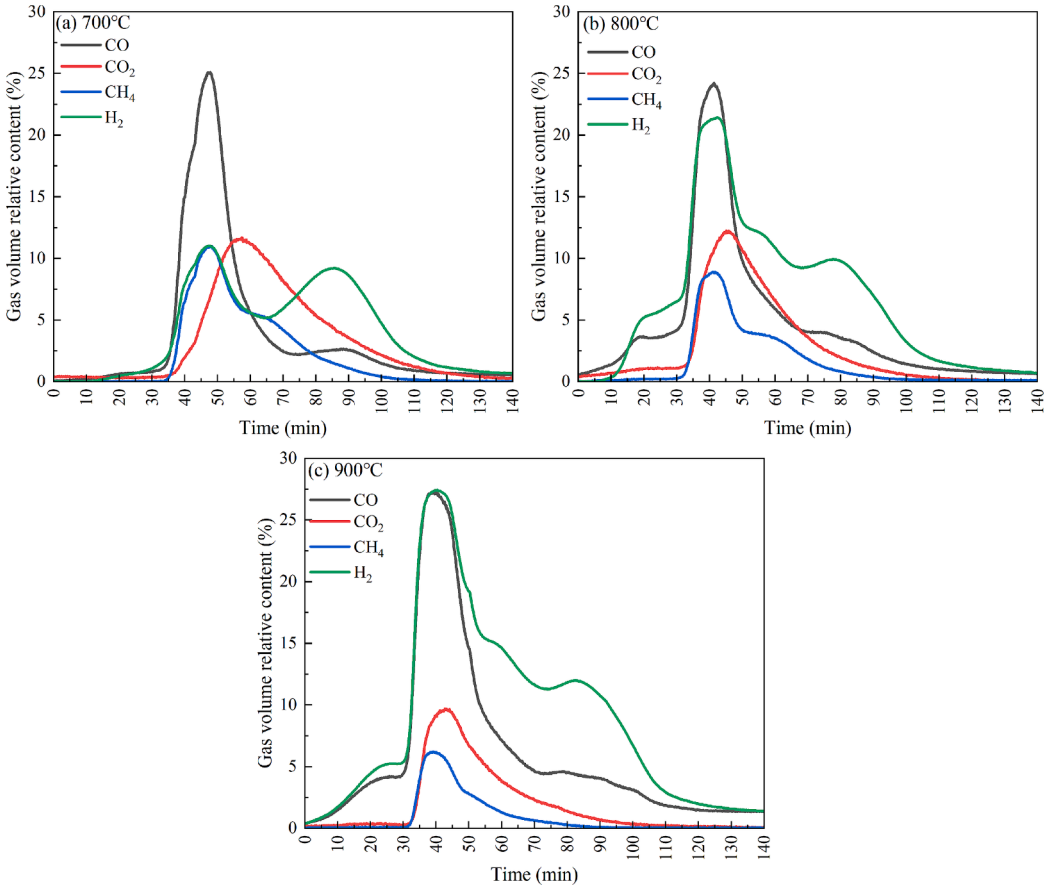

Fig. 6. Effect of catalytic temperature on syngas release curves with biochar.

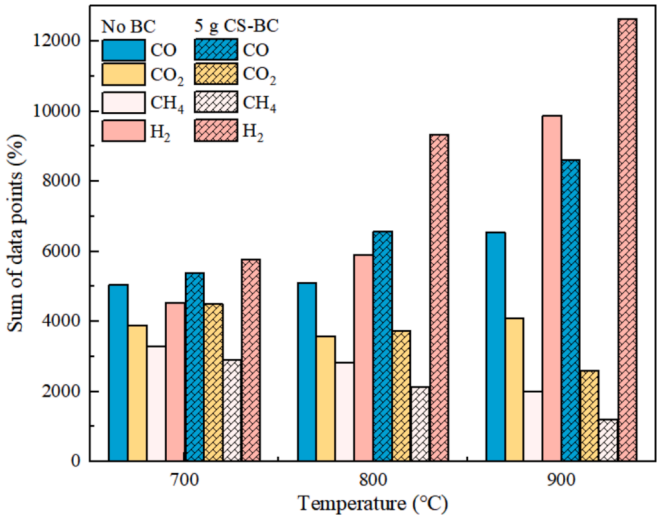

Fig. 7. Effect of catalytic temperature on content of syngas components.

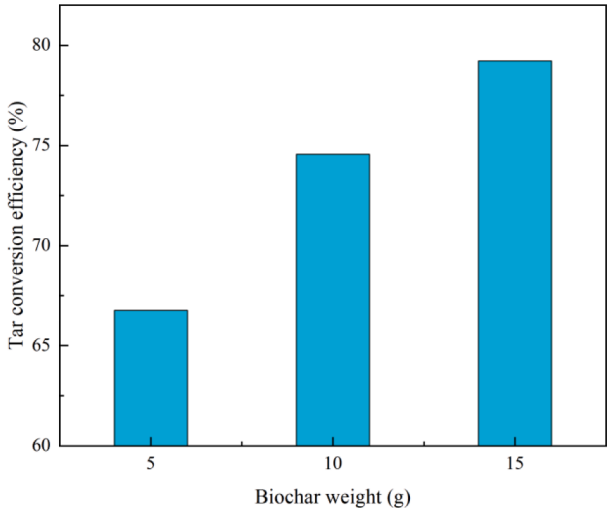

Fig. 8. Effect of biochar mass on tar conversion efficiency.

inhibited the generation of CO_2 and CH_4. In Table S4, as biochar mass increases, the relative content of CH_4 and CO_2 increases, but that of CO_2 and CH_4 reduces. This is mainly because increase of biochar mass extended the reaction time between the gaseous product from biomass pyrolysis and biochar. Also, a larger amount of biochar can provide more active sites to adsorb tar. This further facilitates tar catalytic reforming such as tar cracking, methane steam reforming, Boudouard, water gas reaction, leading to an increase of H_2 and CO and a reduction of CO_2 and CH_4 [32].

3.2.3. *Effect of biochar type on pyrolysis product*

Biochar type affects tar conversion efficiency less than it does catalytic temperature. After catalyzed by the three biochars, the tar conversion efficiencies of wheat stalk are 74.55 %, 72.56 %, and 73.89 %. Among the three biochar catalysts, CS-BC shows good tar conversion efficiency, followed by PS-BC and WS-BC. Fig. 11(b)–(d) show the syngas release curves of wheat stalk after catalyzed by three different biochar catalysts at the biochar mass of 10 g; Fig. 11(a) shows the syngas release curve when wheat stalk is not catalyzed by biochar. After

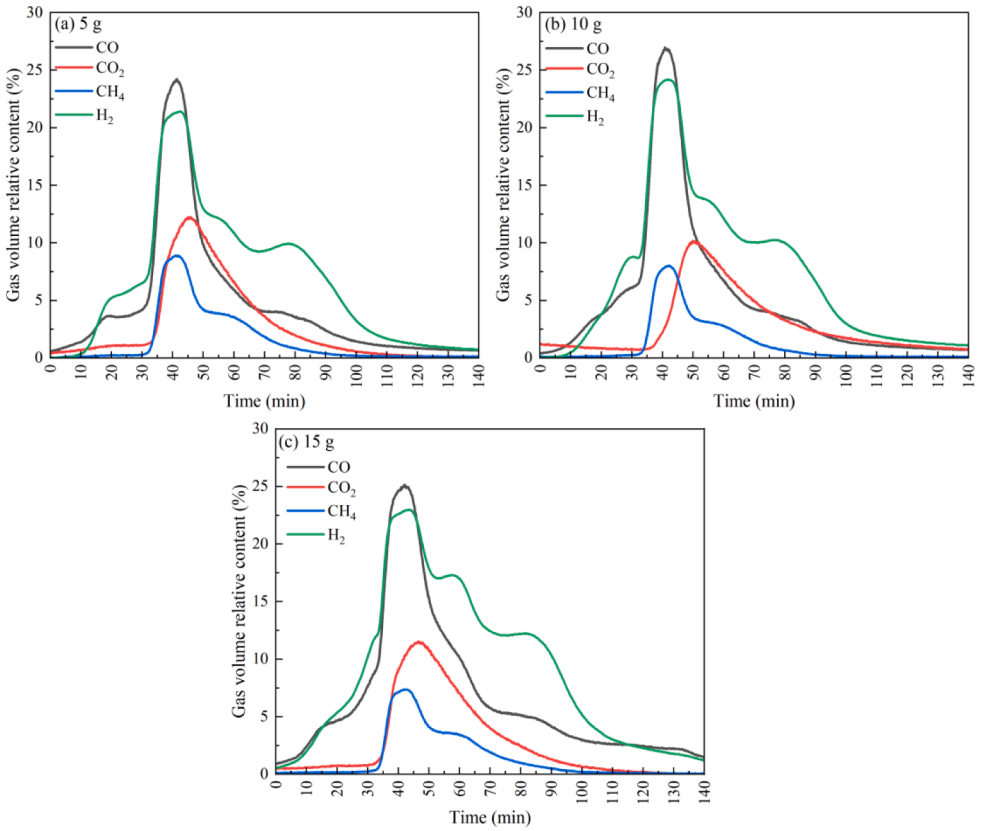

Fig. 9. Effect of biochar mass on syngas release curves.

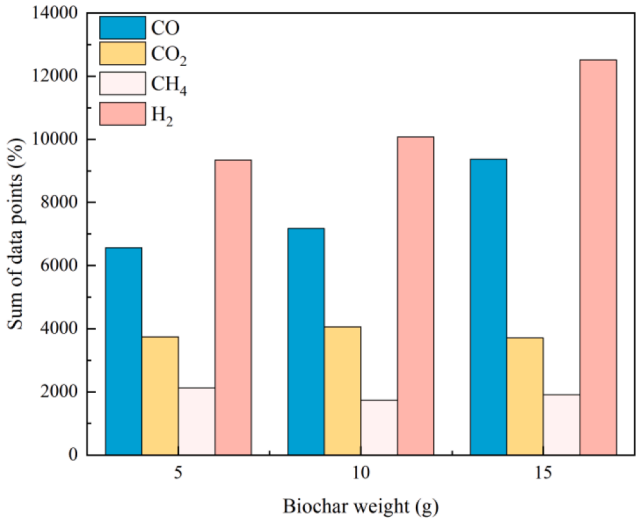

Fig. 10. Effect of biochar mass on content of syngas components.

catalyzed by the three biochars, the maximum values of the H_2 release curve of wheat stalk are 24.17 %, 23.22 %, and 24.81 %, demonstrating minimal difference between different biochars in facilitating hydrogen generation. This minimal difference is associated with surface functional group strength, micromorphology, and specific surface area of biochar. From FTIR analysis, the O-containing functional groups of CS-BC are stronger than those of the other two biochars. The higher tar conversion efficiency after CS-BC catalysis verifies the important role of O-containing functional groups in biochar in catalyzing tar cracking. Also from XRF analysis, the AAEM element content is somewhat different among the three biochars. Presence of AAEM elements K, Ca, Mg, and Na in biochar also helps facilitate tar catalytic cracking, which is more favorable for producing combustible gases like H_2 and CO.

3.2.4. *Effect of activator type on pyrolysis product*

Fig. 12 compares the syngas composition and tar conversion efficiency of wheat stalk for different biochars at the catalytic temperature of 800℃. Activated biochars show high catalytic activity in tar reforming for hydrogen production. Compared with CS-BC, after KBC and HBC catalysis, tar conversion efficiency increased from 66.77 % to 75.26 % and 72.31 %. From the relative volume content of syngas components collected, when activated biochar was used to catalyze tar, more H_2 and CO were generated; KBC facilitated the release of H_2 in syngas better than HBC; HBC facilitated the release of CO in syngas better than KBC. Combining the characterization results of all three catalysts, we can see that the catalytic activity of biochar is closely related to its surface morphology, pore structure, and O-containing functional group. KOH and H_3PO_4 activated biochars are excellent catalysts because activated biochar has more developed surface pore structures, consequently more active sites on the surface; some of the O-containing functional groups of the surface of biochar become stronger. From FTIR analysis, KBC and HBC are different in H_2 generation possibly because of the -OH and other O-containing functional groups in biochar. Addition of an activator changed the composition and contents of metal compounds in biochar. It also affects tar cracking and reforming to a minor degree.

3.2.5. *Effect of activation method on pyrolysis product*

Fig. 13 compares the syngas composition and tar conversion efficiency of biochars prepared with H_3PO_4 by different activation methods after catalyzed at 800℃. Compared with non-activated biochar, both HBC and HBC-2 can improve tar conversion efficiency and facilitate the release of H_2 in syngas. From the tar conversion efficiency and relative content of H_2 in the diagram, the biochar prepared by one step

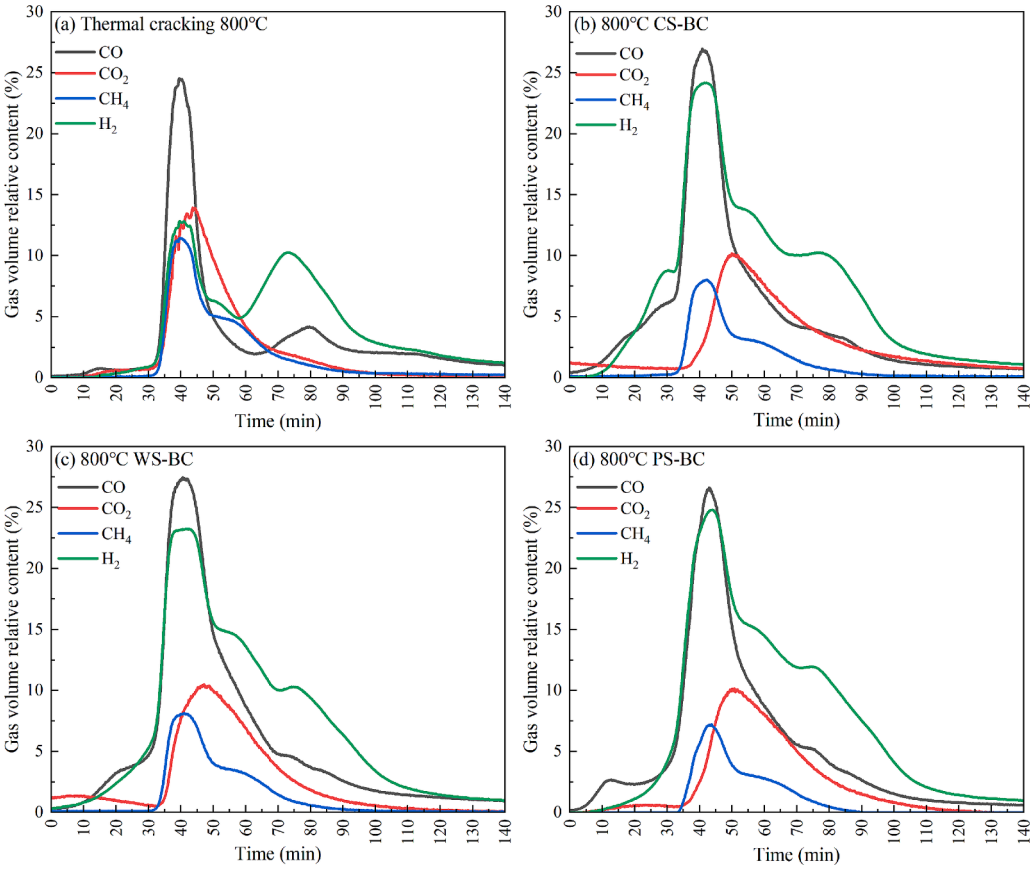

Fig. 11. Syngas release curves of wheat stalk (a) without biochar, (b) with CS-BC, (c) with WS-BC, and (d) with PS-BC.

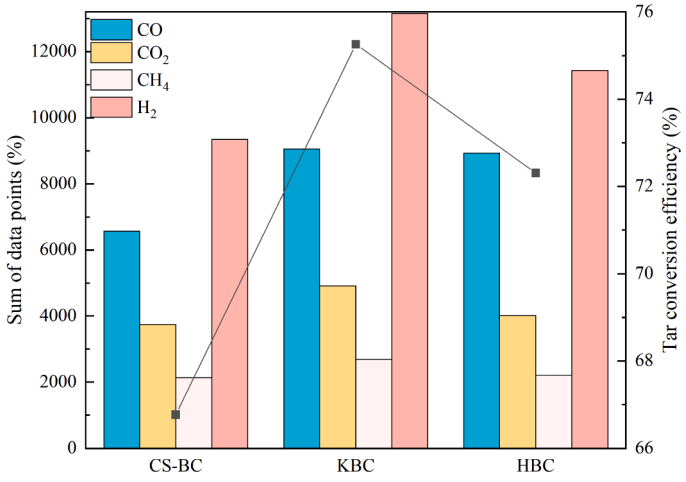

Fig. 12. Syngas and tar conversion efficiency under different activators.

activation is more effective in tar reforming for hydrogen production. This is mainly because the biochar prepared by one step activation is more deeply carbonized and the total mass of the loaded active matter is high. Furthermore, when samples are activated with H_3PO_4 by one step activation, the activator is able to contact directly with the biomass raw material. During impregnation, the activator can easily come into the interior of biomass particles. This facilitates the depolymerization of lignocellulose precursors: partial depolymerization of to lignocellulose can facilitate expansion and pyrolysis reactions [16]. When studying the impregnation of H_3PO_4 with arbor, Jagtoyen *et al.* [33] discovered that H_3PO_4 will begin to react upon exposure to lignocellulose and earlier than hemicellulose and lignin. This confirms that during activation, H_3PO_4 will react with biomass components.

3.2.6. *Effect of biochar catalyst on tar composition*

Fig. 14 shows the GC–MS analysis result of wheat stalk pyrolyzed tar for CS-BC catalyst at 800℃. Table S5 lists some main organics in catalyzed biochar and their relative contents. Compared with when no biochar is used, the content organics components detected by GC–MS is much smaller; the tar composition is much different, too. Fig. 14 compares the color of tar with and without biochar. After biochar catalysis, the tar's color is much lighter, suggesting a reduction in heavy

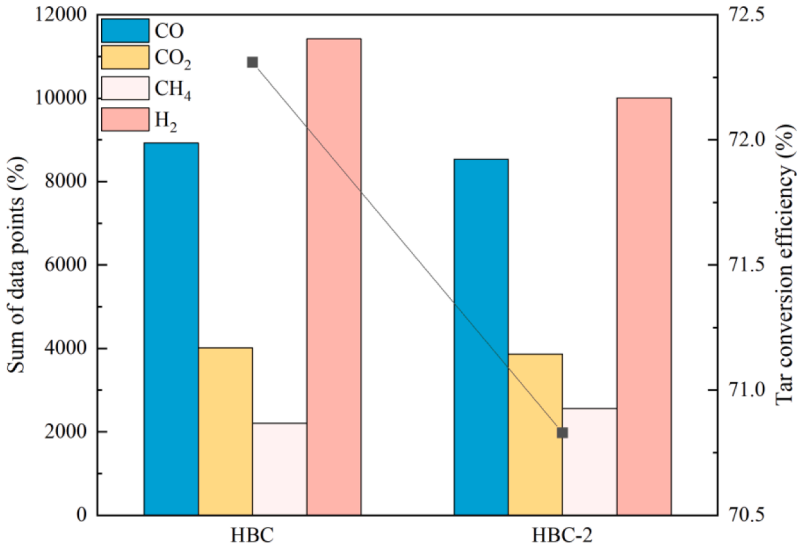

Fig. 13. Syngas and tar conversion efficiency under different activation methods.

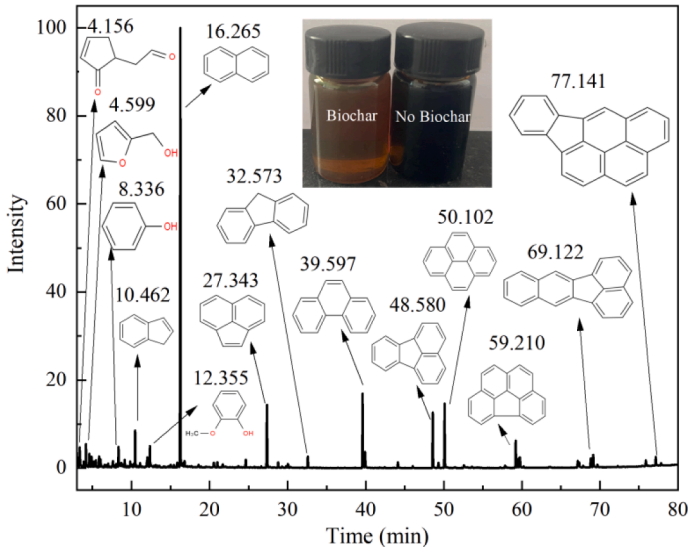

Fig. 14. Organic components in tar after catalysis by CS-BC.

components in tar. When no biochar is added, the tar components are mainly O-containing organics like phenols, furans, and ketones. After biochar is added, although there are still quite a variety of O-containing organics, their relative content is much lower; except phenols, all other O-containing organics have even fully disappeared. During catalytic reaction, O-containing organics are converted into hydrocarbon organics, resulting in an increase in relative content of hydrocarbon organics like naphthalene and cenaphthylene. After biochar catalysis, the relative content of naphthalene in tar is much higher, increasing from 1.19 % to 40.66 %. Shen *et al.* [34] reported similar results when using catalyst to catalyze tar reforming: biochar catalyzed tar is mainly composed of naphthalene; the benzene and toluene in tar will disappear during collection and analysis due to their own volatility. The reduction of relative content of phenols from 4.18 % to 1.99 % and of guaiacol from 9.26 % to 1.59 % also proves that biochar can facilitate the bond breaking and other chemical reactions of O-containing function group structures, converting the O-containing organics in tar into organics containing only O. Both tar appearance and composition confirm that presence of biochar facilitated the reforming of large molecule O-containing organics in tar and greatly reduced the heavy components, whose presence is precisely one of the key drivers behind the clogging and corrosion of biomass pyrolysis-gasification equipment. Sure enough, the ability to convert heavy components in tar into light components and combustible gases after biochar catalysis is very critical to the long, stable operation of biomass pyrolysis-gasification systems.

3.3. *Catalysis mechanism of biochar catalyst*

Fig. 15 shows how biochar catalyzes tar removal. The biochar tar removal path mainly involves adsorption and catalysis. Tar adsorption and catalysis are completed on active sites inside biochar, which are constituted by the variety of O-containing functional groups in biochar, including carboxyl, phenolic hydroxyl, carbonyl, and lactone carboxyl. When they pass biochar, the organics generated from biomass pyrolysis will be adsorbed on the active sites of biochar and then decomposed into radicals. Large molecule organics are even more readily decomposed into radicals under the action of O-containing functional groups. In the meantime, water from pyrolysis will also generate radicals when passing biochar and react with the radicals generated by tar to generate H_2, CO, and small molecule gases. In addition to reactions of organics in biochar,

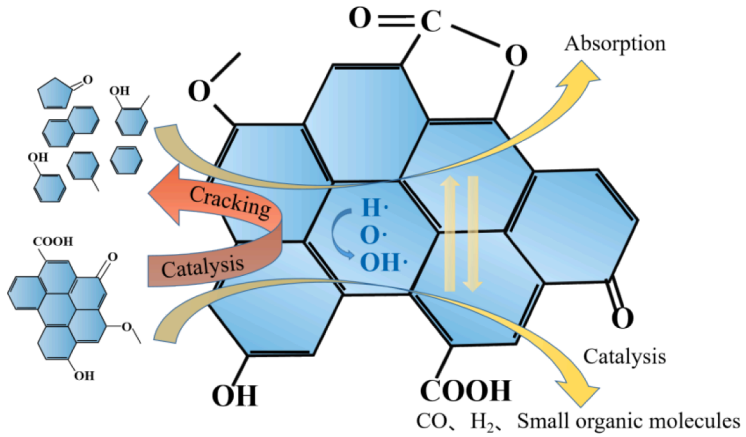

Fig. 15. Tar removal by catalytic cracking with biochar.

chemical reactions—such as Boudouart reaction and water gas reaction—between some inorganics are also involved, leading to an increase in H_2 and CO yield [32]. As catalytic cracking goes on, biochar becomes less able to remove tar. On the one hand, the O-containing functional groups in biochar are gradually reduced. On the other hand, the product from tar cracking will be polymerized into larger molecule aromatic organics, which will gradually turn into carbon deposit to deactivate the catalytic activity of biochar [35]. Singh *et al.* [12] assumed that the adsorption of biochar on tar is mainly targeted at lower molecule aromatic organics, which will be adsorbed in the micropores of biochar by Van der Waals force. Larger molecule aromatic organics take a smaller proportion during adsorption. These organics are adsorbed in the outer pores of biochar.

4. Conclusion

Biochars prepared by pyrolysis include CB-BC, WS-BC, and PS-BC. After catalytic pyrolysis, the tar conversion efficiency and syngas release pattern are similar. Increasing catalytic temperature or catalyst mass helps catalyze tar reforming for hydrogen production; the generation of H_2 is more affected by catalytic conditions at the beginning of pyrolysis. After catalysis, tar mainly contains hydrocarbon organics containing only C and H; the content of O-containing organics is much lower. Also, after catalysis, the amount of heavy components in tar is smaller and the color is much lighter. The different tar catalytic activity among different biochars is related to the micromorphology, surface functional groups, specific surface area, and AAEM element content of tar. Introduction of an activator can make the surface O-containing functional groups richer and the pore structures more developed, which is good for removing tar to generate more H_2. Many micropore structures are generated on the surface of KOH activated tar; the pores on the surface of H_3PO_4 activated tar are larger in size. Tar prepared by one step activation has higher catalytic activity than that prepared by two step activation.

CRediT authorship contribution statement

Jishuo Li: Writing – original draft, Methodology, Investigation, Formal analysis, Data curation, Conceptualization. **Kaili Xu:** Methodology, Conceptualization. **Xiwen Yao:** Writing – review & editing, Validation, Software, Funding acquisition. **Jia Liu:** Investigation, Formal analysis. **Dengke Su:** Software, Investigation, Formal analysis. **Bingchen Wang:** Investigation.

Declaration of competing interest

The authors declare that they have no known competing financial interests or personal relationships that could have appeared to influence the work reported in this paper.

Acknowledgments

This research work was funded by Joint Fund of Natural Science Foundation of Liaoning Province (2023-BSBA-106), Fundamental Research Funds for the Central Universities (N2401021), and Natural Science Foundation of China (52004055).

Appendix A. Supplementary data

Supplementary data to this article can be found online at https://doi.org/10.1016/j.fuel.2025.134862.

Data availability

Data will be made available on request.

References

[1] Meng S, Li W, Li Z, Song H. Recent progress of the transition metal-based catalysts in the catalytic biomass gasification: A mini-review. Fuel 2023;353:129169. https://doi.org/10.1016/j.fuel.2023.129169.
[2] Balasubramanian R, Abishek A, Gobinath S, Jaivignesh K. Alternative fuel : hydrogen and its thermodynamic. Behaviour 2022;3:195–203.
[3] Mladenova E, Slavova M, Abrashev B, Terziev V, Burdin B, Raikova G. Investigation of Ni- and Co-Based Bifunctional Electrocatalysts for Carbon-Free Air Electrodes Designed for Zinc-Air Batteries 2023;7:991–1003.
[4] Tuan T, Sharma P, Jyoti B. ScienceDirect fueling the future : A comprehensive review of hydrogen energy systems and their challenges. Int J Hydrogen Energy 2023;54:791–816. https://doi.org/10.1016/j.ijhydene.2023.08.044.
[5] Abdelhamid HN. ScienceDirect A review on hydrogen generation from the hydrolysis of sodium borohydride. Int J Hydrogen Energy 2020;46:726–65. https://doi.org/10.1016/j.ijhydene.2020.09.186.
[6] Litti YV. ScienceDirect Prospects for the production of green hydrogen : Review of countries with high potential * United States of America Republic of South Africa. Int J Hydrogen Energy 2022;48:4551–71. https://doi.org/10.1016/j.ijhydene.2022.10.084.
[7] Daorattanachai P, Laosiripojana W, Laobuthee A, Laosiripojana N. Type of contribution: Research article catalytic activity of sewage sludge char supported Re-Ni bimetallic catalyst toward cracking/reforming of biomass tar. Renew Energy 2018;121:644–51. https://doi.org/10.1016/j.renene.2018.01.096.
[8] Titirici MM, White RJ, Falco C, Sevilla M. Black perspectives for a green future: Hydrothermal carbons for environment protection and energy storage. Energy Environ Sci 2012;5:6796–822. https://doi.org/10.1039/c2ee21166a.
[9] Cao JP, Liu TL, Ren J, Zhao XY, Wu Y, Wang JX, et al. Preparation and characterization of nickel loaded on resin char as tar reforming catalyst for biomass gasification. J Anal Appl Pyrolysis 2017;127:82–90. https://doi.org/10.1016/j.jaap.2017.08.020.
[10] Wang Y, Huang L, Zhang T, Wang Q. Hydrogen-rich syngas production from biomass pyrolysis and catalytic reforming using biochar-based catalysts. Fuel 2022;313:123006. https://doi.org/10.1016/j.fuel.2021.123006.
[11] Song Y, Wang Y, Hu X, Hu S, Xiang J, Zhang L, et al. Effects of volatile-char interactions on in situ destruction of nascent tar during the pyrolysis and

gasification of biomass. Part I. Roles of nascent char. Fuel 2014;122:60–6. https://doi.org/10.1016/j.fuel.2014.01.002.
[12] Singh S, Kumar Bhaumik S, Dong L, Li CZ, Vuthaluru H. An integrated two-step process of reforming and adsorption using biochar for enhanced tar removal in syngas cleaning. Fuel 2022;307:121935. https://doi.org/10.1016/j.fuel.2021.121935.
[13] Wijitkosum S. Influence of Pyrolysis Temperature and Time on Biochar Properties and Its Potential for Climate Change Mitigation 2023;4:472–85.
[14] Ashok J, Dewangan N, Das S, Hongmanorom P, Wai MH, Tomishige K, et al. Recent progress in the development of catalysts for steam reforming of biomass tar model reaction. Fuel Process Technol 2020;199:106252. https://doi.org/10.1016/j.fuproc.2019.106252.
[15] Peng H, Gao P, Chu G, Pan B, Peng J, Xing B. Enhanced adsorption of Cu(II) and Cd (II) by phosphoric acid-modified biochars. Environ Pollut 2017;229:846–53. https://doi.org/10.1016/j.envpol.2017.07.004.
[16] Nakagawa Y, Molina-Sabio M, Rodríguez-Reinoso F. Modification of the porous structure along the preparation of activated carbon monoliths with H3PO4 and ZnCl2. Microporous Mesoporous Mater 2007;103:29–34. https://doi.org/10.1016/j.micromeso.2007.01.029.
[17] Benedetti V, Ail SS, Patuzzi F, Cristofori D, Rauch R, Baratieri M. Investigating the feasibility of valorizing residual char from biomass gasification as catalyst support in Fischer-Tropsch synthesis. Renew Energy 2020;147:884–94. https://doi.org/10.1016/j.renene.2019.09.050.
[18] Liang S, Guo F, Du S, Tian B, Dong Y, Jia X, et al. Synthesis of Sargassum char-supported Ni-Fe nanoparticles and its application in tar cracking during biomass pyrolysis. Fuel 2020;275:117923. https://doi.org/10.1016/j.fuel.2020.117923.
[19] Burke GM, Wurster DE, Berg MJ, Veng-Pedersen P, Schottelius DD. Surface characterization of activated charcoal by X-ray photoelectron spectroscopy (XPS): correlation with phenobarbital adsorption data. Pharm Res An Off J Am Assoc Pharm Sci 1992;9:126–30. https://doi.org/10.1023/A:1018900431661.
[20] Yang H, Chen Z, Chen W, Chen Y, Wang X, Chen H. Role of porous structure and active O-containing groups of activated biochar catalyst during biomass catalytic pyrolysis. Energy 2020;210:118646. https://doi.org/10.1016/j.energy.2020.118646.
[21] Liu Y, Paskevicius M, Wang H, Parkinson G, Veder JP, Hu X, et al. Role of O-containing functional groups in biochar during the catalytic steam reforming of tar using the biochar as a catalyst. Fuel 2019;253:441–8. https://doi.org/10.1016/j.fuel.2019.05.037.
[22] Chen W, Fang Y, Li K, Chen Z, Xia M, Gong M, et al. Bamboo wastes catalytic pyrolysis with N-doped biochar catalyst for phenols products. Appl Energy 2020;260:114242. https://doi.org/10.1016/j.apenergy.2019.114242.
[23] Shen Y, Yoshikawa K. Tar conversion and vapor upgrading via in situ catalysis using silica-based nickel nanoparticles embedded in rice husk char for biomass pyrolysis/gasification. Ind Eng Chem Res 2014;53:10929–42. https://doi.org/10.1021/ie501843y.
[24] Xu C, (Charles), Hamilton S, Ghosh M. Hydro-treatment of Athabasca vacuum tower bottoms in supercritical toluene with microporous activated carbons and metal-carbon composite. Fuel 2009;88:2097–105. https://doi.org/10.1016/j.fuel.2009.05.020.
[25] Klinghoffer NB, Castaldi MJ, Nzihou A. Influence of char composition and inorganics on catalytic activity of char from biomass gasification. Fuel 2015;157:37–47. https://doi.org/10.1016/j.fuel.2015.04.036.
[26] Wu FC, Tseng RL, Juang RS. Preparation of highly microporous carbons from fir wood by KOH activation for adsorption of dyes and phenols from water. Sep Purif Technol 2005;47:10–9. https://doi.org/10.1016/j.seppur.2005.03.013.
[27] Guo Y, Rockstraw DA. Physicochemical properties of carbons prepared from pecan shell by phosphoric acid activation. Bioresour Technol 2007;98:1513–21. https://doi.org/10.1016/j.biortech.2006.06.027.
[28] Castro-Muñiz A, Suárez-García F, Martínez-Alonso A, Tascón JMD. Activated carbon fibers with a high content of surface functional groups by phosphoric acid activation of PPTA. J Colloid Interface Sci 2011;361:307–15. https://doi.org/10.1016/j.jcis.2011.05.064.
[29] 7He 1Nfluence 0F 7Empera7Ure and Hea71N6 Ra7E 0N 7He 5L0W Pyr0Ly515 0F 810Ma55 1996;1481:6–7.
[30] Hantoko D, Su H, Yan M, Kanchanatip E, Susanto H, Wang G, et al. Thermodynamic study on the integrated supercritical water gasification with reforming process for hydrogen production: Effects of operating parameters. Int J Hydrogen Energy 2018;43:17620–32. https://doi.org/10.1016/j.ijhydene.2018.07.198.
[31] Park J, Lee Y, Ryu C, Park YK. Slow pyrolysis of rice straw: Analysis of products properties, carbon and energy yields. Bioresour Technol 2014;155:63–70. https://doi.org/10.1016/j.biortech.2013.12.084.
[32] Zhang L, Yao Z, Zhao L, Li Z, Yi W, Kang K, et al. Synthesis and characterization of different activated biochar catalysts for removal of biomass pyrolysis tar. Energy 2021;232:120927. https://doi.org/10.1016/j.energy.2021.120927.
[33] Jagtoyen M, Derbyshire F. Activated carbons from yellow poplar and white oak by H3PO4 activation. Carbon N Y 1998;36:1085–97. https://doi.org/10.1016/S0008-6223(98)00082-7.
[34] Shen Y, Zhao P, Shao Q, Ma D, Takahashi F, Yoshikawa K. In-situ catalytic conversion of tar using rice husk char-supported nickel-iron catalysts for biomass pyrolysis/gasification. Appl Catal B Environ 2014;152–153:140–51. https://doi.org/10.1016/j.apcatb.2014.01.032.
[35] Dong L, Asadullah M, Zhang S, Wang XS, Wu H, Li CZ. An advanced biomass gasification technology with integrated catalytic hot gas cleaning Part I. Technology and initial experimental results in a lab-scale facility. Fuel 2013;108:409–16. https://doi.org/10.1016/j.fuel.2012.11.043.